Supporting Information

Philip et al. 10.1073/pnas.0903092107

SI Text

Additional Computational Studies of Electronic Transitions in the *p*CA Chromophore of PYP. A number of additional computational studies regarding electronic transitions in PYP have been reported (1–3). These studies focus on the energy gap between the S_0 and S_1 states.

Involvement of Multiple Vibrational Modes. We consider the case that two vibrational modes are coupled to the optical transition under study. This complication has been examined extensively in the case of stillbene (4). The S_0 and S_1 energy surfaces are now two-dimensional and are often approximated using two harmonic oscillators for the two vibrational modes involved. Franck-Condon factors now require the determination of the overlap of S_0 and S_1 wave functions in this space. The simplest case is that of ΔE-tuning, in which the energy gap between the S_0 and S_1 energy surfaces is altered. In this case the predictions for the spectral effects remain unchanged compared to those for a single vibrational mode. If changes in the spectra involve R_e-tuning, different cases need to be considered. If the change in equilibrium nuclear geometry is limited to a single vibrational mode, again the spectral predictions remain unchanged. However, it is possible that changes in R_e occur along both vibrational modes, and that these two shifts are in opposite directions. Thus, these two changes in the energy surfaces would have opposite effects on the spectra. In the qualitative approach followed here, this would be expected to result in very small spectral changes that would be insufficient to explain the large changes in λ_{max}^{abs} from 441 to 478 nm observed in the E46X set of mutants. Thus, R_e-tuning would only make a significant contribution to explaining the observed spectra if the shifts in R_e along one of the vibrational modes dominate the spectral effects (or if the changes in R_e along the two modes are in the same direction). In this case the vibrational mode along which the dominant shift in R_e occurs results in unchanged qualitative predictions for the spectra. Similar considerations apply to the case of W-tuning. If compensating changes in W occur along the two vibrational modes, this will result in a minimal contribution of W-tuning to the experimentally observed spectra. Only if the change in W along one vibrational mode is dominant (or if the shifts in W along the two axes are in the same direction, for example both involving an increase in the W of the S_1 state), will this type of tuning be observed in the spectra, according to the qualitative predictions derived for the single oscillator case.

The above arguments remain valid if additional vibrational modes are considered. We conclude that the qualitative predictions based on the involvement of a harmonic well (i.e., a single vibrational mode) remain qualitatively valid if multiple vibrational modes are coupled to the optical transition. These considerations also reveal that if compensating spectral tuning effects occur along different vibrational modes, these will be largely spectrally silent, and can therefore not be derived from measurements of the electronic absorbance and fluorescence emission spectra.

Spectral Tuning Due to Inhomogeneous Broadening Caused by Heterogeneity in *p*CA Configuration. We consider the possibility that some of the changes in peak position, peak width, and peak asymmetry observed in the E46X mutants of PYP are caused by inhomogeneous broadening of the spectral bands due to heterogeneity in *p*CA configuration. This possible explanation of the spectral changes induced by the mutations implies that the various substitutions at position 46 have differential effects on the heterogeneity in *p*CA configuration. For example, it may be that one mutation causes heterogeneity in the strength of one of the active site hydrogen bonds known to cause spectral tuning, and results in a red-shift in λ_{max}^{abs}. Another mutation may cause a change in the distribution of dihedral angles that describe the configuration of the *p*CA molecule in its protein binding pocket, and may result in a blue-shift in λ_{max}^{abs}. We consider this possibility in the light of three experimental observations: that the values for λ_{max}^{fl} are largely unaltered while the values for λ_{max}^{abs} are strongly affected in the E46X mutants (Fig. 5), that the changes in the shape of the absorbance spectra are much larger than those for the fluorescence emission spectra (Fig. 4 *B* and *C*), and that a clear correlation is observed between the position and the width of the spectral bands (Fig. S1). These three patterns in the data would not be expected if heterogeneity in *p*CA configuration would be a major contributor to the observed spectral tuning effects. In the two examples described above, spectral tuning caused by structural heterogeneity in active site hydrogen bonding strength and *p*CA dihedral angle would not be expected to leave the position or shape of the fluorescence emission spectrum largely unchanged, or to change the width of the fluorescence emission spectrum according to a simple pattern. We conclude that the three stated regularities in the data argue against a major contribution of heterogeneity in *p*CA configuration to the spectral tuning effects observed in the E46X mutants.

Spectral Effects of Increased Width of S_1 Energy Surface. We attribute the larger width of the PYP absorbance spectra compared to its fluorescence emission spectra to the increased width of the S_1 energy surface compared to that of the S_0 state based on the following reasoning. The intensity of electronic transitions from the S_0 state to higher vibrational levels in the S_1 state tends to become increasingly weak. This is caused by the closely spaced features of positive and negative amplitude in the corresponding S_1 wave function, which are prone to cancel out net overlap with the much broader wave function for the vibrational ground state of S_0. In the case that the S_1 energy surface becomes broader, the spacing of positive and negative features of the wave functions of all vibrational levels will become larger. This will tend to result in a larger net positive overlap between the S_0 vibrational ground state and S_1 vibrationally excited wave functions, and therefore an increase in the Franck-Condon factors for transitions to higher vibrational levels of S_1. This will result in contributions to the absorbance spectrum of transitions to a larger number of vibrational levels in the S_1 state and a broadened absorbance band.

Arguments Against R_e Tuning in the E46X Mutants. Changes in R_e would result in two effects. First, it would cause λ_{max}^{abs} and λ_{max}^{fl} to be anticorrelated. This effect is not observed in the data (Fig. 5). Second, the shape of the absorbance and fluorescence emission spectra would be significantly and similarly altered. We used two measures to quantify the shape of the absorbance and emission spectra of the E46X mutants: the width of the spectra at 3/4 height and the asymmetry of the spectral bands. The width and asymmetry of the absorbance spectra change by a factor 2.05 and 2.35, respectively, in the E46X mutants. These values are 1.36 and 1.35 for the fluorescence emission spectra. This analysis demonstrates that the changes in shape of the absorbance spectra are significantly larger than those in the emission spectra in the E46X mutants. Thus, we conclude that substitutions at position 46 do not cause significant changes in

the difference between the R_e values for the S_0 and S_1 states of the *p*CA chromophore in PYP.

Effects of Substitutions on *p*CA Charge Distribution and W of S_1. Substitutions of Glu46 to Arg, Lys, Asp, and Pro cause a blue-shift of the λ_{max}^{abs}, corresponding to a broadening of the S_1 energy surface. All other substitutions (except Tyr) cause red-shifts (particularly Ile, Val, Met, and Leu) (5), corresponding to a narrowing of S_1. How do these substitutions alter the W of the S_1 state? One possibility for the latter set of mutants is that the removal of the short, strong hydrogen bond between the side chain of Glu46 and the deprotonated phenolic oxygen of the *p*CA in wt PYP (6) is involved. The loss of this hydrogen bond in the mutants could alter the force constants of vibrational modes in the *p*CA that are coupled to the optical transition, resulting in a change in the W of the S_1 energy surface. Since the *p*CA chromophore in PYP is a charged molecule buried within the protein, changes in hydrogen bonding or the vicinity of charged side chains can significantly alter the charge distribution of the *p*CA, either in the S_0 or S_1 state. The formation of the S_1 state results in a large charge redistribution in the *p*CA (7), and a slight weakening of the hydrogen bond between Glu46 and the *p*CA (8). Thus, the removal of the hydrogen bond between the phenolic oxygen of the *p*CA and residue 46 in the mutants is likely to affect the W of the S_0 and S_1 states differently. Particularly the bond order of the isomerizing C – C bond in the *p*CA molecule could be affected by a change in excited state charge distribution caused by the mutations. In this proposal the charged residues Arg, Lys, and Asp would have an effect on *p*CA charge distribution—and thus C – C bond order—in the S_1 state opposite to that of weakening of the hydrogen bond between residue 46 and the *p*CA: the Arg and Lys substitutions could reduce conjugation in the chromophore by localizing electrons on the phenolic oxygen of the *p*CA, while the Asp substitution would result in charge localization on its carbonyl oxygen. Typical C – C stretching and C = C stretching frequencies of 1,150 and $1,550\ cm^{-1}$ yield an estimation for the change in C – C bond order of $\sim 100\ cm^{-1}$ as the factor responsible for observed changes in λ_{max}^{abs} in the E46X mutants. The involvement of a vibrational mode with this frequency in the absorbance spectrum of PYP is supported by the vibrational fine structure of PYP ($\sim 1,300\ cm^{-1}$) reported from low temperature studies (9), the observation that a band at $1,558\ cm^{-1}$ is the strongest signal in the resonance Raman spectrum of PYP (10), and the involvement of a mode at $1,550\ cm^{-1}$ in the optical transition of stillbene (4).

Mutagenesis and Batch Purification of PYP. Mutagenesis of PYP was performed with primers degenerate at position 46 (5′-ATC CTT CAG TAC AAC GCC GCG **NNN** GGC GAC ATC ACC GGC CGC GAC-3′ and complement) as described in ref. 5. A pQE-80A plasmid (QIAGEN) containing the *pyp* gene inserted between *Bam*HI and *Hin*dIII sites was used as the template. All mutants were confirmed by DNA sequencing and transformed into *E. coli* BL21. Colonies of the 20 *E. coli* strains were grown in deep-well microplates and induced with 1 mM IPTG.

For batch purification *E. coli* BL21 containing the pQE80-PYP plasmid was grown in overnight cultures that were used to inoculate 1.5 L expression cultures the following day. These were grown at 37 °C to an optical density at 600 nm of 0.6. IPTG was added to a final concentration of 1 mM. After 4–5 h, the cells were harvested by centrifugation at 4,000 g for 20 min. At this point the cells could be frozen at −80 °C for use at a later time. Otherwise they were resuspended in 3–5 mL of lysis buffer (50 mM NaH_2PO_4, 500 mM NaCl, 5 mM imidazole, pH 8.0). Lysozyme was added to a concentration of 1 mg/mL and the mixture was incubated on ice for 30 min. The cells were broken by sonication and the cellular debris was spun down at 10,000 g for 30 min. The supernatant was collected and the PYP was reconstituted with chromophore by adding pCA (p-coumaric acid) anhydride (11) until the visible absorbance peak was no longer observed to increase. NH_4SO_4 was added to 50% saturation. The precipitate was spun down at 20,000 g for 15 min. The supernatant was collected and dialyzed with lysis buffer. Afterwards this was mixed with 5–15 mL of 50% Ni-NTA agarose suspension (QIAGEN) and stirred for 1 h at 4 °C. The agarose suspension was poured into a column and washed with lysis buffer containing 10 mM imidazole. The protein was eluted from the column with an imidazole step gradient. The sample was then applied onto a DEAE Sepharose Fast Flow (Amersham) column and eluted with a NaCl gradient. After that a third purification step was performed using gel filtration chromatography with Superdex 200 in an HK 16/60 column (Amersham).

Ultrafast Pump-Probe Spectroscopy. We used a homebuilt 2 kHz amplified Ti:sapphire laser system, which produces 50 fs, 50 μJ pulses centered at 800 nm. In the pump-probe measurements, the pump beam was obtained by second-harmonic generation in a 200 μm thick Type-I beta barium borate (BBO) crystal (Quantum Technology). A tunable probe beam is produced with an optical parametric amplifier (OPA) yielding 10–50 nJ, 80–90 fs pulses tunable from 450–520 nm. The pump and probe pulses were compressed and precompensated for material dispersion from transmissive optics in the pump-probe setup using separate prism compressors. A 30 cm focal length spherical mirror and a 20 cm focal length achromatic lens were used to focus the pump (100 nJ) and probe (~5 nJ) pulses. For all pump-probe experiments, the sample was contained in a spinning cell rotated at 10 Hz and had a 0.2 mm path length. For wt PYP and E46Y PYP a 400 nm probe beam was used; for wt PYP and the E46K and E46Y mutants probe beams at 490 nm, 505 nm, and 515 nm were used; finally E46H PYP was probed at 505 nm.

1. Sergi A, Gruning M, Ferrario M, Buda F (2001) Density functional study of the photoactive yellow protein's chromophore. *J Phys Chem B* 105:4386–4391.
2. Groenhof G, Lensink MF, Berendsen HJC, Snijders JG, Mark AE (2002) Signal transduction in the photoactive yellow protein. I. Photon absorption and the isomerization of the chromophore. *Proteins Struct Funct Genet* 48:202–211.
3. He Z, Martin CH, Birge R, Freed KF (2000) Theoretical studies on excited states of a phenolate anion in the environment of photoactive yellow protein. *J Phys Chem A* 104:2939–2952.
4. Chiang W-Y, Laane J (1994) Fluorescence spectra and torsional potential functions for *trans*-stillbene in its S_0 and S_1 (π, π^*) electronic states. *J Phys Chem* 100:8755–8767.
5. Philip AF, Eisenman KT, Papadantonakis GA, Hoff WD (2008) Functional tuning of photoactive yellow protein by active site residue 46. *Biochemistry* 47:13800–13810.
6. Anderson S, Crossoon S, Moffat K (2004) Short hydrogen bonds in photoactive yellow protein. *Acta Crystallogr D* 60:1008–1016.
7. Premvardhan LL, van der Horst MA, Hellingwerf KJ, van Grondelle R (2003) Stark spectroscopy on photoactive yellow protein, E46Q, and a nonisomerizing derivative, probes photo-induced charge motion. *Biophys J* 84:3226–3239.
8. Groot ML, van Wilderen LJGW, Larsen DS, van der Horst MA, van Stokkum IHM, Hellingwerf KJ, van Grondelle R (2003) Initial steps of signal generation in photoactive yellow protein revealed with femtosecond mid-infrared spectroscopy. *Biochemistry* 42:10054–10059.
9. Hoff WD, Kwa SLS, Van Grondelle R, Hellingwerf KJ (1992) Low temperature absorption and fluorescence spectroscopy of the yellow protein from *Ectothiorhodospira halophila*. *Photochem Photobiol* 56:529–539.
10. Kim M, Mathies RA, Hoff WD, Hellingwerf KJ (1995) Resonance Raman evidence that the thioester-linked 4-hydroxycinnamyl chromophore of photoactive yellow protein is deprotonated. *Biochemistry* 34:12669–12672.
11. Imamoto Y, Ito Y, Kataoka M, Tokunaga, F (1995) Reconstitution of photoactive yellow protein from apoprotein and *p*-coumaric acid derivatives. *FEBS Lett* 374:157–160.

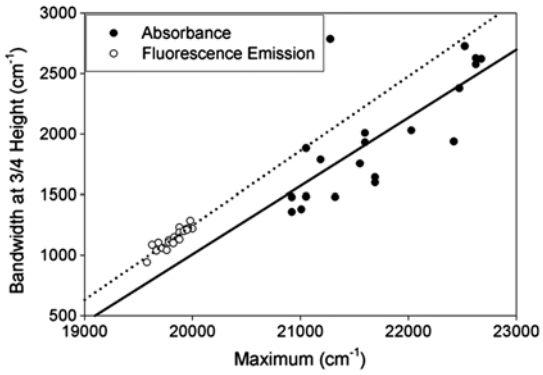

Fig. S1. Correlations between maximum and bandwidth of the absorbance (black circles) and fluorescence emission (open circles) spectra of the E46X mutants.

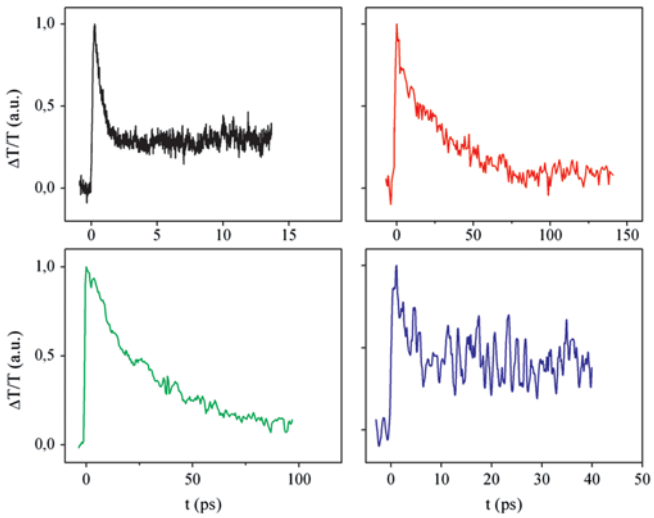

Fig. S2. Sub-ps transient absorbance pump-probe spectroscopy of wt PYP (black line) and its E46H (blue line), E46K (green line), and E46Y (red line) mutants.

Table S1. Summary of the properties of the E46X mutants reported here

Substitution	λ^{abs}_{max} (nm)	λ^{abs}_{max} (cm^{-1})	Abs BW	Abs Asymm	λ^{fl}_{max} (nm)	λ^{fl}_{max} (cm^{-1})	Fl Em BW	Fl Asymm	Φ_{fl}	Stokes Shift
A	469	21,322	1,480	0.76	507	19,724	1,059	1.14	0.55	1,598
C	472	21,186	1,787	0.48	504	19,831	1,149	1.03	0.64	1,355
D	442	22,624	2,575	0.55	501	19,960	1,221	0.84	0.79	2,664
E	446	22,422	1,937	0.58	501	19,980	1,284	0.97	0.19	2,442
F	470	21,277	2,785	0.33	503	19,881	1,230	1.06	1.05	1,396
G	463	21,598	2,007	0.36	504	19,861	1,132	1.13	0.66	1,737
H	454	22,026	2,027	0.43	502	19,940	1,215	1.06	0.62	2,086
I	478	20,921	1,357	0.67	510	19,627	1,086	0.95	0.56	1,293
K	444	22,523	2,725	0.78	503	19,881	1,188	1.03	1.27	2,642
L	475	21,053	1,484	0.64	509	19,666	1,038	0.99	0.44	1,387
M	476	21,008	1,379	0.70	511	19,579	942	1.10	0.39	1,429
N	463	21,598	1,929	0.44	505	19,822	1,100	1.06	0.60	1,777
P	441	22,676	2,620	0.49	501	19,950	1,210	0.91	0.85	2,726
Q	461	21,692	1,598	0.63	506	19,763	1,041	1.07	0.37	1,929
R	442	22,624	2,626	0.48	502	19,920	1,200	1.00	0.98	2,704
S	464	21,552	1,754	0.54	506	19,782	1,107	1.02	0.54	1,769
T	475	21,053	1,882	0.38	506	19,782	1,123	1.10	0.61	1,270
V	478	20,921	1,478	0.52	508	19,685	1,103	1.00	0.53	1,235
W	461	21,692	1,642	0.49	503	19,881	1,130	1.03	0.65	1,811
Y	445	22,472	2,377	0.52	500	20,000	1,220	1.07	1.44	2,472
Averages	461	21,712	1,973	0.54	504	19,826	1,139	1.03	0.69	1,886